LA-UR- 09-07711

Approved for public release; distribution is unlimited.

Title:	Diamond Photodiodes for X-ray Applications
Author(s):	James R. Distel, ISR-1 John Smedley, BNL Jeffrey W. Keister, BNL Erik Muller, Stony Brook University Jean Jordan-Sweet, IBM T.J. Watson Research Center Jen Bohon, Case Western Reserve University Bin Dong, Global Stategies Group North America
Intended for:	Material Research Society (MRS) Fall Meeting 2009

Los Alamos
NATIONAL LABORATORY
EST. 1943

Form 836 (7/06)

Diamond Photodiodes for X-ray Applications.

J. Smedley[1]; *J. W. Keister*[1]; *E. Muller*[3]; *J. Jordan-Sweet*[5]; *J. Bohon*[6]; *J. Distel*[2]; *B. Dong*[4]
[1]Brookhaven National Laboratory, Upton, NY, USA.
[2]Los Alamos National Laboratory, Los Alamos, NM, USA.
[3]Stony Brook University, Stony Brook, NY, USA.
[4]Global Strategies Group, North America, Crofton, MD, USA.
[5]IBM T.J. Watson Research Center, Yorktown Heights, NY, USA.
[6]Center for Synchrotron Biosciences, Case Western Reserve University, Upton, NY, USA.

ABSTRACT

Single crystal high purity CVD diamonds have been metallized and calibrated as photodiodes at the National Synchrotron Light Source (NSLS). Current mode responsivity measurements have been made over a wide range (0.2-28 keV) of photon energies across several beamlines. Linear response has been achieved over ten orders of magnitude of incident flux, along with uniform spatial response. A simple model of responsivity has been used to describe the results, yielding a value of 13.3±0.5 eV for the mean pair creation energy. The responsivity vs. photon energy data show a dip for photon energies near the carbon edge (284 eV), indicating incomplete charge collection for carriers created less than one micron from the metallized layer.

INTRODUCTION

Diamond is an attractive material for x-ray windows and transmission x-ray monitors due to its low Z and good thermal properties. Diamond also has application in high radiation environments as an x-ray sensor [1-4]. However, only recently has material become commercially available with low enough impurity and defect density to realize its potential in radiometric applications such as synchrotron diagnostics and scientific instrumentation [5]. The present report describes the observation of calculable diode responsivity under controlled conditions, as measured at several NSLS synchrotron beamlines, spanning a wide range of photon energies and flux levels. Methods of metallization and surface preparation will be discussed, along with the effect of thermal annealing on these contacts.

METALLIZATION and SURFACE PREPARATION

Several methods of creating electrical contacts on diamond have been investigated. These can be broken into three broad categories – metal contacts on oxygen-terminated diamonds, thermally annealed contacts using carbide-forming metals, and annealed contacts using non-carbide forming metals. The process used to create each of these contacts will be described in this section, along with physical analysis of the contacts.

All of the devices discussed herein begin with single crystal "detector grade" material obtained from Element6. These plates are typically 4x4 mm^2 and 0.25-0.5 mm thick with a [001] surface orientation and a [110] edge normal. The surface finish has been measured with atomic force microscopy and found to be consistent with the manufacturer's specification of < 4 nm roughness. Prior to metallization, the plates are treated with a standard chromic acid etch to both remove surface non-diamond carbon and leave the surface oxygen terminated. Subsequent oxygen termination has also been achieved via exposure to an ozone lamp for several hours. Near-edge x-ray absorption fine structure (NEXAFS) oxygen-edge analysis has verified that both methods are capable of producing an oxygen-terminated surface.

Metal contacts, typically ~30 nm thick, are formed via sputtering. A mask is used to create a 3 mm diameter contact on the center of both sides of the diamond. Several metals have been investigated on oxygen-terminated diamond – copper, platinum, niobium, molybdenum, and titanium (with a platinum capping layer). In all cases, prior to thermal annealing, the contacts were found to be blocking – meaning that they did not support photoconductive gain/persistent photocurrent, and there exists a bias beyond which the response is independent of field.

Thermal annealing was used on some samples to demonstrate the creation and properties of carbide contacts and to prepare detectors which were intended to operate in high flux (and resulting high temperature) environments. NEXAFS analysis indicates that temperatures above 600 °C cause loss of oxygen termination; this leads to injecting contacts for all metals tested, however the extent and location of the resulting photoconductive gain varies greatly with contact. For high-flux x-ray irradiation, it is the temperature that the detector reaches, and not the irradiation, which causes the loss of oxygen and subsequent change in the contact nature. To investigate this, a sample was irradiated with focused white beam at NSLS beamline X28C (100 W/cm^2 with an energy range of 5-15 keV) for 1 min; oxygen edge NEXAFS showed no change in the oxygen-edge feature due to this irradiation.

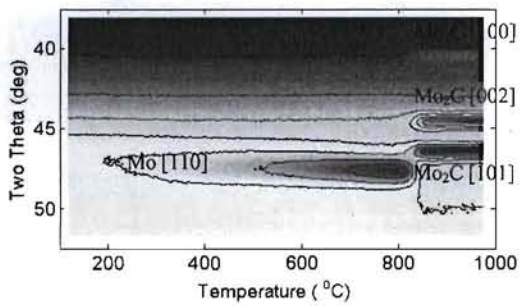

Figure 1. Annealing of Mo contact to form Mo_2C. Color scale provides peak intensity.

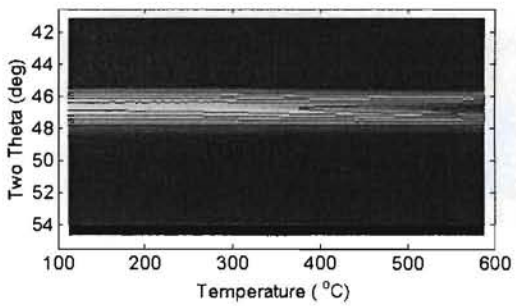

Figure 2. Annealing of Pt contact showing [111] texture growth.

Annealing was performed in a He-filled oven with *in-situ* x-ray diffraction at beamline X20C. For carbide forming metals, this capability allows the formation of the carbide to be directly observed and the transition temperature to be measured. Figure 2 shows the formation of Mo_2C contacts on diamond, starting from a 30 nm Mo film. The ramp rate is 3 °C/s, and the transition temperature is 835 °C. For Pt contacts intended for high flux applications, annealing in the x-ray diffraction (XRD) oven reveals a significant increase in grain size above 400 °C. This film has a [111] fiber texture which strengthens upon heating. The peaks become significantly narrower during annealing, indicating an increase in grain size. Subsequent Scherrer analysis of the diffracting grain size via high-resolution XRD at X20A revealed that the pre-anneal [111] fiber-textured grain size was ~50 Å, and the post anneal size was ~200 Å. Other random texture components had smaller grain sizes, down to 26 (pre-anneal) and 70 (post-anneal) Å.

DETECTOR CALIBRATION

Calibration of detectors has been performed across five NSLS beamlines – U3C, X6B, X8A, X15A and X28C. Together, these sources provide photon energies from 200 eV to 28 keV and flux from 100 pW to 10 W, with beam diameters from 20 μm to 2 mm. Calibration is done via comparison to a silicon photodiode at low flux and soft/tender x-rays, an ion chamber at mid

flux, and a copper calorimeter at the highest flux. One side of a detector is biased, and the other is used for charge collection. Both pulsed and DC biases are used; here pulsed bias is a square wave defined by a duty cycle and frequency as well as amplitude and polarity. Current through the detector is monitored using Keithley electrometers (models 617 & 6517). For the soft x-ray lines (U3C and X8A), the detectors are calibrated in vacuum; all other calibrations are performed in ambient conditions, with the exception of high flux testing at X28C, where a dry N_2 environment is used to limit ozone production.

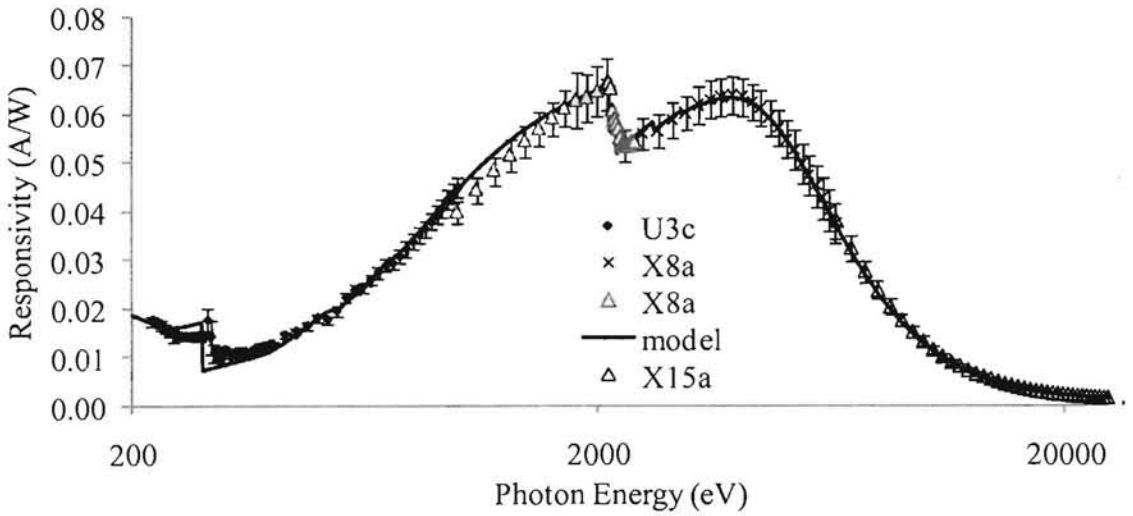

Figure 3 – Responsivity vs. photon energy for a 260 μm thick oxygen-terminated diamond with 40 nm thick platinum contacts. 200 V bias on incident electrode was used (hole bias), with 1 kHz, 95% duty cycle for energies up to 1 keV and 100% duty cycle beyond 1 keV.

Figure 3 shows the responsivity of a diamond with blocking platinum contacts (on oxygen terminated diamond) as a function of incident photon energy for positive bias on the incident electrode. In the soft x-ray regime, we refer to this as hole mode, as the current is carried primarily by holes pushed away from the incident electrode and collected on the transmission side. Beyond 4 keV, this distinction no longer holds, as the photons are absorbed (and thus carriers are created) throughout the thickness of the diamond. Note that the flux of the various beamlines used to create figure 3 varies widely with photon energy; thus the fact that the responsivity follows a predictable theory (see discussion for details on the model) implies that the diamond response is linear in flux over the range of 100 pW to 10 μW. High flux measurements have extended this linearity up to 1 W [6], but under these conditions the blocking nature of the contact is lost due to heating. Below 1 keV photons, a pulsed bias is used to enable full collection. This is necessary to prevent the buildup of trapped charge; carriers produced by the beam during the "off" portion of the cycle drift under the influence of the trapped charge, eventually neutralizing it. For hole bias, full collection can be achieved with up to 99% duty cycle at 0.1 MV/m (25 V across a 0.25 mm thick diamond). For electron transport, trapping is a more significant problem, and higher fields or smaller duty cycles are required. Figure 4 shows the responsivity vs. bias for both polarities with 1 keV photons (the bias is on the incident electrode, thus the "hole" bias is positive and the "electron" bias is negative). The spatial uniformity of detectors with blocking contacts is excellent – figure 5 shows a spatial response map with 19 keV photons taken at X15A under +200 V bias. The circular area corresponds to the

metalized region of the device, while the notch at the bottom comes from the mount used to hold the diamond. The x-ray beam used for the map is 0.2x0.2 mm^2. The area of increased response near the mount is an artifact of x-rays striking the copper holder. The scale is referenced to the expected response of 2.2 mA/W at this photon energy.

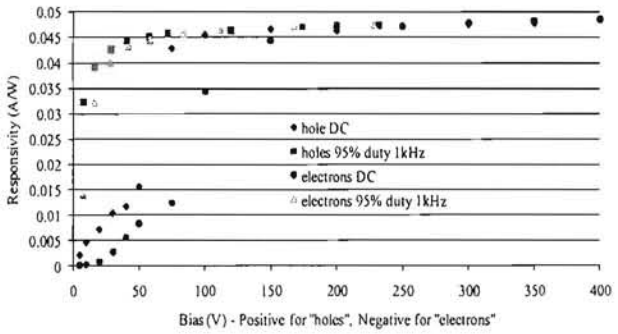

Figure 4 – Responsivity vs. Bias for diamond from fig. 3, for 1 keV photons.

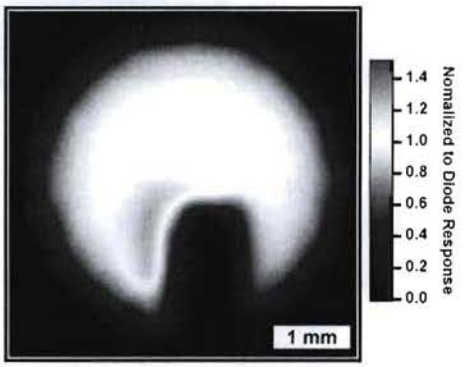

Figure 5 – Response map for diamond from fig. 3, with 19 keV photons and +200 V bias.

For carbide contacts, the situation is significantly different, especially for electron bias. These contacts support charge injection and photoconductive (PC) gain. Figure 6 shows the bias dependence of responsivity for an annealed diamond with a Ti/Pt contact. For hole bias (99% duty cycle), this dependence looks similar to that of blocking contacts (fig. 4), with full hole collection at a field of 0.1 MV/m - indicating that the hole charge collection distance is equal to the thickness of the diamond at this field. The electron transport for low fields is significantly less than the expected value, indicating charge trapping. For fields > 0.1 MV/m, the responsivity is significantly *greater* than expected, because the trapped electrons lead to hole injection. These injected holes cross the diamond many times before the electrons are detrapped or the holes are themselves trapped. This can only occur for field at which the hole charge collection distance is greater than the thickness of the material (this explains why there is no gain below 0.1 MV/m). Above this value, the gain should be roughly linear with bias, as the hole velocity is linear with bias in this regime. The responsivity vs. photon energy for a 0.3 mm thick diamond with annealed Ti/Pt contacts is shown in figure 7 for three bias conditions.

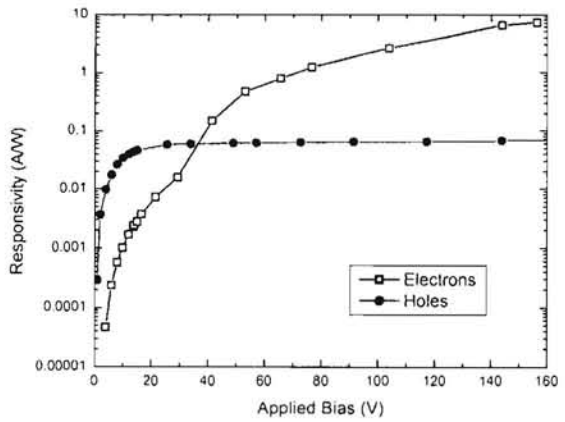

Figure 6 – Responsivity vs bias for a diamond with annealed Ti/Pt contacts; 1 keV photons.

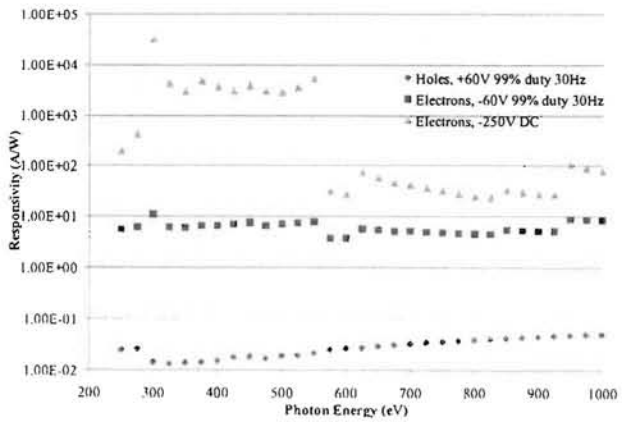

Figure 7 – Responsivity vs. photon energy for diamond from fig. 6.

The beamline flux increases by two orders of magnitude from 550 eV to 600 eV. This change is evident in the electron response, especially for DC bias, demonstrating that PC gain is non-linear with flux. For hole bias, however, the response is similar to the blocking case (fig. 3), again suggesting that electron trapping is the cause of the PC gain. For carbide contacts, gain occurs everywhere that electrons are incident on the contact. Figure 8 shows response maps of a diamond with an injecting Mo_2C contact on one side and an injecting Mo contact on the other side. These maps were taken at 19 keV, so both carriers are moving throughout the material. PC gain is observed at all points when the bias is set to move electrons toward the Mo_2C contact - every point in the metalized area is at least 5 times the expected response; some areas are much higher. For the opposite bias, the gain is much lower, and is observed only in isolated areas (similar to the annealed platinum discussed below).

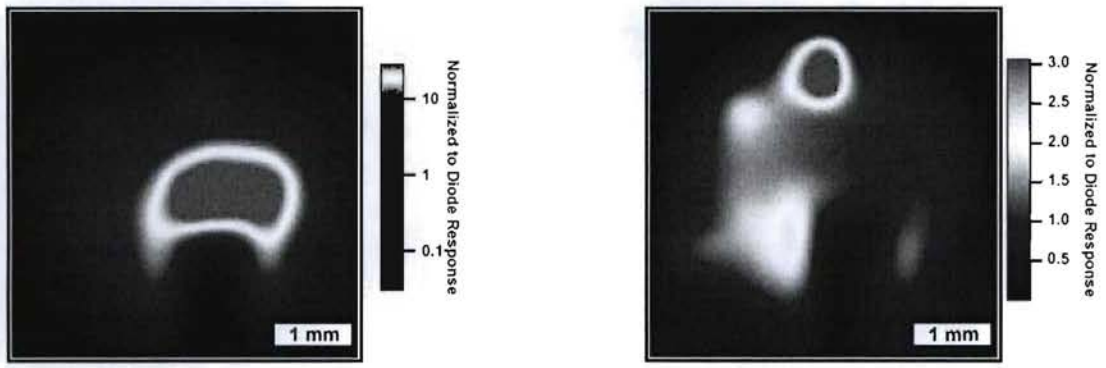

Figure 8 – Spatial response maps for a diamond with one carbide contact. Note the difference in color scale. The map on the left, with the diamond biased (-200 V DC) to move electrons toward the Mo_2C contact, shows gain over the entire metalized region. The map on the right, with the opposite bias (+200 V) shows significantly lower and more isolated PC gain.

Annealed platinum contacts are also injecting, but PC gain occurs only at locations where defects appear in x-ray topographs of the material (specifically single-point strain fields associated with inclusions). In contrast to the carbide contacts, these areas of gain are typically only ~100 um across, and some diamonds with low defect density show very few of these spots.

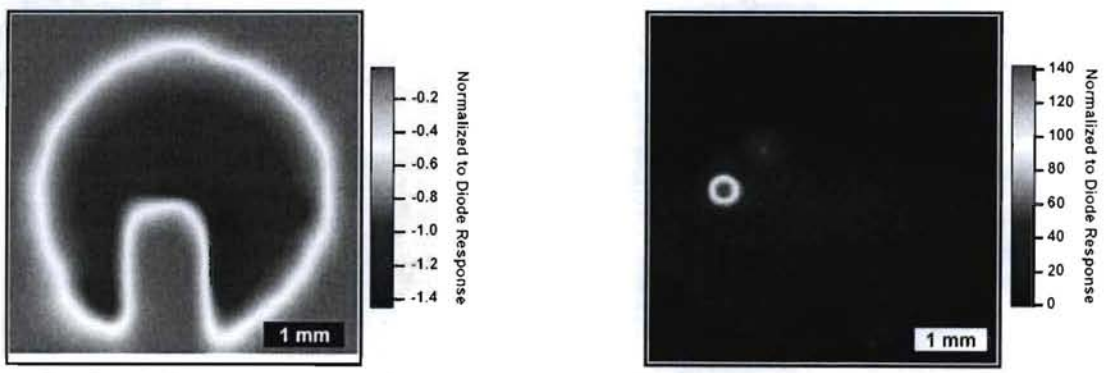

Figure 9 – Spatial response maps for a diamond with annealed platinum contacts, for both -200V (left) and +200 V (right) bias. PC gain in observed only in two locations, and only for + bias.

Figure 9 shows response maps of a diamond with annealed Pt contacts under positive and negative bias at 19 keV. PC gain occurs at different locations for each polarity, leading us to conclude that the feature responsible for the charge trapping must be near the hole injecting electrode to cause gain. Away from these defect regions, the annealed Pt contacts behave similarly to the blocking contacts, providing predictable, diode like response. Once the contact is annealed, its behavior remains consistent at any flux level – diamonds with annealed Pt contacts have been shown to be linear with a dynamic range of *11 orders of magnitude.*

DISCUSSION and CONCLUSIONS

The responsivity (S) of the diamonds with blocking contacts (or annealed contacts away from PC regions) is predictable by a simple expression:

$$S[\nu] = (\frac{1}{w})(e^{-\frac{t_{metal}}{\lambda_{metal}[\nu]}})(1 - e^{-\frac{t_{dia}}{\lambda_{dia}[\nu]}})CE[\nu, F]$$

Here w is the mean ionization energy of diamond; for these measurements, 13.25±0.5 eV has been obtained [5]. t_{dia} and t_{metal} are the thickness of the diamond and the metal, and λ_{dia} and λ_{metal} are the photon-energy dependent absorption lengths of the diamond and the metal. CE represents the collection efficiency of the device. For most photon energies, CE is unity as long as the field (F) is sufficient for full collection. For photons near the carbon K edge (284 eV), the carriers are created very near the incident electrode (under 100 nm); this leads to loss of carriers due to diffusion into the metal layer. CE is obtained by empirical fit to monte carlo results [7]. This is the source of the carbon edge feature in fig. 4; this feature is bias dependent, unlike the absorption feature at 2120 eV which results from the platinum M edge. The parameters for model curve in fig. 4 (platinum contacts) were w=13.8 eV, t_{Pt} = 40 nm, t_{dia} = 260 microns.

We have demonstrated that diamond can be used to create calibrated photodiodes for x-ray applications. It is important to both choose appropriate contact materials for a given environment and to be aware that pulsed biasing may be required to achieve full carrier collection, particularly for soft x-ray applications.

ACKNOWLEDGMENTS

The authors wish to thank John Walsh for design and fabrication of sample mounts and Xiangyun Chang for assistance with metallization. The team is further indebted to Veljko Radeka, Pavel Rehak, Peter Siddons, Triveni Rao, Dimitre Dimitrov and Ilan Ben-Zvi for discussion and guidance over the course of this work. The authors wish to acknowledge the support of the U.S. Department of Energy under grant DE-FG02-08ER41547. This manuscript has been authored by Brookhaven Science Associates, LLC under Contract No. DE-AC02-98CH10886 with the U.S. Department of Energy.

REFERENCES

1. D. R. Kania, L. S. Pan, P. Bell, et al., J. Appl. Phys. 68 (1) (1990) 124.
2. H. Pernegger, S. Roe, P. Weilhammer, et al., J. Appl. Phys. 97 (7) (2005) 073704.
3. H. Kagan, Nucl. Instr. and Meth. Phys. Res. Sect. A 541 (1-2) (2005) 221.
4. P. Bergonzo, D. Tromson, C. Mer, J. Synch Radiat. 13 (2006) 151.
5. J. W. Keister and J. Smedley, Nucl. Instr. and Meth. Phys. Res. Sect A 606 (2009) 774.
6. J. Bohon et al., these proceedings.
7. D. Dimitrov et al., these proceedings